View metadata, citation and similar papers at core.ac.uk

brought to you by CORE

provided by Caltech Authors

PROCEEDINGS OF SPIE

SPIEDigitalLibrary.org/conference-proceedings-of-spie

Terrestrial exoplanet coronagraph image quality: study of polarization aberrations in Habex and LUVOIR update

J. B. Breckinridge, M. Kupinski, J. Davis, B. Daugherty, R. A. Chipman

J. B. Breckinridge, M. Kupinski, J. Davis, B. Daugherty, R. A. Chipman, "Terrestrial exoplanet coronagraph image quality: study of polarization aberrations in Habex and LUVOIR update," Proc. SPIE 10698, Space Telescopes and Instrumentation 2018: Optical, Infrared, and Millimeter Wave, 106981D (6 July 2018); doi: 10.1117/12.2311880

SPIE.

Event: SPIE Astronomical Telescopes + Instrumentation, 2018, Austin, Texas, United States

Downloaded From: https://www.spiedigitallibrary.org/conference-proceedings-of-spie on 7/18/2018 Terms of Use: https://www.spiedigitallibrary.org/terms-of-use

Terrestrial exoplanet coronagraph image quality polarization aberrations in Habex[♦,#]

J. B. Breckinridge[1, 2], M. Kupinski[1], J. Davis[1], B. Daugherty[1] and R. A. Chipman[1]
1. College of Optical Sciences, University of Arizona, Tucson, AZ
2. California Institute of Technology, Pasadena, CA.

ABSTRACT

Direct imaging and spectroscopy of terrestrial exoplanets requires the control of vector electromagnetic fields to approximately one part in ten to the fifth over a few milliarc second FOV to achieve the necessary 10^{-10} intensity contrast levels. Observations using space telescopes are necessary to achieve these levels of diffracted and scattered light control. The highly reflecting metal mirrors and their coatings needed to image these very faint exoplanets introduce polarization into the wavefront, which, in turn affects image quality and reduces exoplanet yield unless corrected. To identify & create the technologies and the electro-optical/mechanical-spacecraft systems models that will achieve these levels, NASA is currently developing two mission concepts, each with their own hardware vision. These are: The Habex, a habitable planet explorer and the LUVOIR, a Large Ultra-Violet Optical-Infrared space telescope system.

This paper reports the results of polarization ray-tracing the HabEx detailed optical prescription provided by the project to the authors in the fall of 2017. Diattenuation and retardance across both the exit pupil associated with the occulting mask and the exit pupil associated with the coronagraph image plane are given as well as the corresponding Jones pupil matrices. These are calculated assuming isotropic coatings on all mirrors. Analysis and physical measurements indicates that the specification of the primary mirror for exoplanet coronagraphs will need to include a constraint on spatially varying polarization reflectivity (anisotropic coatings).

The Jones exit-pupil phase terms, phi XX and phi YY just before the occulting mask differ in shape and are displaced one from the other by about 10 milli-waves. This shows that A/O, which corrects for geometric path differences, cannot completely correct for wavefront errors introduced by polarization for this particular prescription for HabEx. We suggest that these differences may be corrected by adjusting the opto-mechanical design to change angles of incidence on mirrors and corrected by adjusting the design of the dielectric coatings on the highly-reflecting mirror surfaces. Super-posing the phase of XX onto the phase of YY and then correcting using A/O will assure maximum power transmittance through the system and best contrast. These aspects require further investigation.

Keywords: Exoplanet, coronagraph, polarization aberration, HabEx, telescopes, coatings, physical optics

♦ Paper 10698-48 on 13 June 2018 • 10:30 - 10:50 AM | SPIE Astronomical Telescopes + Instrumentation, Austin TX
Work partially supported by NASA contract NNX17AB29G awarded by SMD exoplanet program office under TDEM15 to the College of Optical Sciences, University of Arizona, Tucson

Space Telescopes and Instrumentation 2018: Optical, Infrared, and Millimeter Wave, edited by Makenzie Lystrup, Howard A. MacEwen, Giovanni G. Fazio, Proc. of SPIE Vol. 10698, 106981D
© 2018 SPIE · CCC code: 0277-786X/18/$18 · doi: 10.1117/12.2311880

Downloaded From: https://www.spiedigitallibrary.org/conference-proceedings-of-spie on 7/18/2018
Terms of Use: https://www.spiedigitallibrary.org/terms-of-use

1. INTRODUCTION

An optical system corrected for geometric path difference errors is a necessary but not sufficient condition for the perfect image formation needed to directly image terrestrial exoplanets. Geometric (trigonometric) path difference errors are controlled using adaptive optics (tip-tilt & wavefront), active metrology and precision pointing. However, image quality is also determined by several physical optics factors: diffraction, polarization, partial coherence, and chromatism all of which degrade image quality and are not corrected through the control of geometric path difference by adaptive optics. The source of physical optics errors lies in the opto-mechanical packaging of optical elements, masks, stops and the thin film coatings needed to obtain high system transmittance.

Breckinridge Kuper & Shack[1] (1984) analyzed the use of the Lyot coronagraph to image distant exoplanets and modeled an optical system using the scalar approximation to the vector electromagnetic wave. They showed how scalar-complex apodization of the exit pupil reveals an exoplanet in the presence of mirror fabrication errors. Breckinridge & Oppenheimer[2] showed that internal polarization plays an important role in exoplanet coronagraphy. Recently, Breckinridge[3] and Chipman[4] used vector E&M wave analysis with the polarization aberration tools developed by Chipman and others to model point-spread functions (PSF) for astronomical telescopes and discovered that several physical optics effects are in reality very important for the design of the high-performance coronagraphs needed for direct imaging and spectroscopy of terrestrial exoplanets.

Today, ground and space exoplanet coronagraphs are designed and built under the assumption that the scalar wave approximation to the vector electromagnetic wave[5,6], is adequate. Balasubramanian et. al. [7] examined a terrestrial planet finder (TPF) coronagraph design using vector electromagnetic (E&M) waves and concluded that for TPF designs vector-waves were not necessary to develop a system to control unwanted background radiation to the level required at that time.

In this paper, we present the optical-polarization model of HabEx. This text is divided into 8 sections. Section 1 is the introduction.-Section 2 presents the principles of scalar-wave image formation. Section 3 describes image formation in the presence of polarization. Section 4 describes polarization ray-trace. Section 5 describes the principles of the Lyot coronagraph for exoplanet science, Section 6 presents the polarization properties of HabEx in the absence of the vector vortex mask[8]. Section 7 describes a particular A/O challenge for HabEx, Section 8 presents measurements made by Brian Daugherty of form birefringence from a large (4-meter) mirror, coated to ground-based astronomical standards, and Section 9 presents conclusions.

2. SCALAR WAVE IMAGE FORMATION

In this section, we provide a brief review of image formation modeled using scalar wave theory as a basis to extend the work into the more accurate vector representation.

Object space irradiance distribution can be decomposed into an ensemble of delta functions. The intensity or height of each delta function maps out the structure of the object. The optical system operates on the complex amplitude and phase associated with that intensity distribution to form an image at the detector. Most astronomical sources in the visible region of the spectrum radiate broadband, incoherent thermal light.

The theory of image formation is developed using the schematic shown in Figure 2 below. The coordinate system we use in our analysis is shown in Fig 2 below. This system is in standard use by modern textbooks[ix,x] on the physics of image formation. Light travels left to right. The object plane to the left (#1 in the system) is represented by Cartesian coordinates from the Latin alphabet x_1, y_1 the pupil plane (#2 in the System) is represented by Cartesian coordinates from the Greek alphabet ξ_2, η_2 and the image plane (#3 in the System) is represented by Cartesian coordinates from the Latin alphabet x_3, y_3.

Downloaded From: https://www.spiedigitallibrary.org/conference-proceedings-of-spie on 7/18/2018
Terms of Use: https://www.spiedigitallibrary.org/terms-of-use

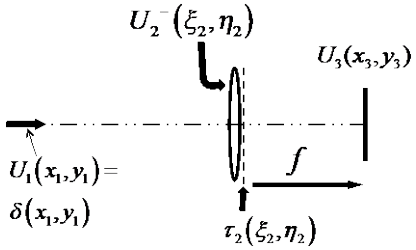

Figure 1 schematic of an optical system in the meridional plane. The object space complex field $U_1(x_1,y_1)$ is shown as a delta function $\delta(x_1,y_1)$ to represent a star on-axis. This object space field is propagated by Fresnel diffraction to just to the left of the entrance pupil and is shown by $U_2^-(\xi_2,\eta_2)$. The pupil is shown to have a complex transmittance $\tau_2(\xi_2,\eta_2)$ at plane 2. The optical system, shown here schematically has a lens of focal length f, and provides the optical power to create the field $U_3(x_3,y_3)$ at an image plane 3.

The scalar complex amplitude and phase across the image plane is found by standing at the image plane (#3) in Fig 1 and looking to the left, or back through the system toward the object. The Fresnel-Kirchoff diffraction integral is used to model the propagation of scalar electromagnetic waves through the optical system shown in Fig. 2. The complex amplitude and phase field $U_3(x_3,y_3)$ at the image plane is given by

$$U_3(x_3,y_3)= \mathbf{K}\int_{-\infty}^{\infty}\int_{-\infty}^{\infty}[U_2^-(\xi_2,\eta_2)]\cdot\tau_2(\xi_2,\eta_2)\cdot\exp\left\{-j\frac{2\pi}{\bar{\lambda}f}(x_3\xi_2+y_3\eta_2)\right\}d\xi\,d\eta \qquad \text{Eq. 1}$$

Where K is a constant, the integral is taken over the complex field across the exit pupil, $U_2^-(\xi_2,\eta_2)$ of the optical system whose focal length is f, $\bar{\lambda}$ is the quasimonochromatic wavelength of light. Eq 1 is written for the scalar wave solution to Maxwell's equations and the not vector wave solution to Maxwell's equation. The amplitude and phase complex properties across the exit pupil are contained in the scalar term,

$$\tau_2(\xi_2,\eta_2)=A_2(\xi_2,\eta_2)\exp\{i\phi_2(\xi_2,\eta_2)\} \qquad \text{Eq. 2}$$

Where $A_2(\xi_2,\eta_2)$ varies between 0 and 1 and describes amplitude part of the complex wave as a function of position across the exit pupil. The phase properties at each point across the exit pupil are described by $\phi_2(\xi_2,\eta_2)$.

To the left in Fig 2, we have a point source represented by a delta function. This point source is mapped onto the image plane. We record intensity at the image plane and define the image plane irradiance distribution for this point source to be:

$$PSF_{\text{Scalar Diffraction}} \equiv |U_3(x_3,y_3)|^2. \qquad \text{Eq. 3}$$

Next if we let the object space irradiance be represented by $I_{\text{Object}}(x_1,y_1)$ and the image space irradiance represented by $I_{\text{Image}}(x_3,y_3)$ and use the theoretical development of Goodman, we can write,

$$I_{\text{Image}}(x_3,y_3)=I_{\text{Object}}(x_1,y_1)\otimes PSF, \qquad \text{Eq. 4}$$

Where the symbol $\otimes$ denotes the convolution operator.

The analysis above reviews the classical scalar approach to modeling optical systems. Our new approach, needed for high contrast optical systems is to model white-light electromagnetic radiation as a vector. To understand the need for vector-wave physical optics, we need to review the source of polarized light within an optical system and understand the complex (amplitude and phase) wavefront at the focal plane $U_3(x_3,y_3)$ where coronagraphers place the occulting mask to control scattered light to one part in 10^{11}.

Downloaded From: https://www.spiedigitallibrary.org/conference-proceedings-of-spie on 7/18/2018
Terms of Use: https://www.spiedigitallibrary.org/terms-of-use

3. IMAGE FORMATION IN THE PRESENCE OF POLARIZATION

The vector-wave (polarization) aspect of light plays two major roles in exoplanet coronagraphy. One is the application of polarimetry to extract scientific information of value about the physical nature of the source and the other is telescope/instrument induced polarization effects on system transmittance, image quality and coronagraph instrument contrast.

Polarimetry

Polarimetry is the science and measurement of the polarization properties of light. It is performed by making relative radiometric measurements of the intensity of the source (image) as it passes through each of three polarization filters and the image of the same source that passes through no filter. From these four intensity measurements we calculate the Stokes parameters at multiple points across the image. Proto-planetary systems exhibit primordial gas and dust that, after time, will form exoplanets. Polarization measurements at different points across the gas and dust cloud reveal particle sizes and preferred orientation to help explain planetary system formation and evolution. Exoplanets themselves are not resolved by telescopes and therefore their image is the point spread function of the telescope/coronagraph system.

All telescope/coronagraphs introduce their own "noise" polarization into the signal. Space telescope/coronagraph architectures need to minimize this "noise" and maximize system transmittance. This will enable us to calibrate the instrument polarization in order to separate instrument polarization from the source polarization. Many authors discuss methods to calibrate photopolarimetric measurements for changes in polarization transmissivity[11,12].

Instrument polarization

The work presented in the remainder of this report concentrates on the polarization properties of the HabEx telescope/coronagraph system as represented by the September 2017 end-to-end optical prescription provided by the program office.

A thought experiment using linear orthogonal polarizers and a telescope shows the role of vector waves in image formation and, by implication, the effects of polarization on contrast. Figure 1 shows the effects of adding unwanted polarizers to an optical system: Top left shows an open, unmasked exit pupil of a telescope with zero geometric wavefront error. Top right shows the shape of the PSF recorded with the pupil on the top left. Bottom left shows the same telescope pupil as that shown in the upper left, but now with two linear polarizers over the top, each aligned orthogonal to the other. In the lower left of Fig 1, we see that horizontally polarized light is admitted to the left-hand side of the pupil and vertically polarized light is admitted to the right-hand side of the pupil. The bottom right shows the PSF recorded using the pupil on the bottom left. Note that with no polarizer (top of Fig 2) the angular resolution is not position-angle dependent, however, with the polarizers (bottom of Fig 2) the angular resolution is position angle dependent. Astronomers define the angle between two objects as "position angle". It is the rotation angle in the plane of the sky, or in this case the plane of object space. That is, the upper right in Figure 1 shows that the angular resolution is the same in all directions from the axis, whereas the lower right in Figure 1 the angular resolution is not the same in all directions from the system axis. Angular resolution in the vertical direction exceeds that in the horizontal direction for the PSF shown in the lower right.

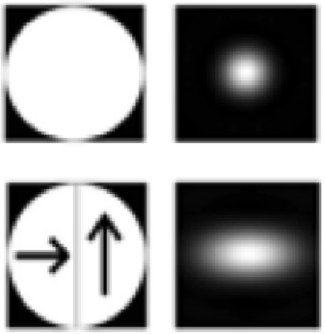

1.

Figure 2 PSF's shown for a telescope with zero geometric wavefront aberration without (upper) and with (lower) polarizers. Note that the shape of the PSF changes and thus shape of the mask needed to attenuate the radiation changes.

Downloaded From: https://www.spiedigitallibrary.org/conference-proceedings-of-spie on 7/18/2018
Terms of Use: https://www.spiedigitallibrary.org/terms-of-use

We give the physical optics explanation for this phenomenon. Orthogonally polarized white light does not interfere to create an image. In Fig 1, the lower left image of the exit pupil the polarized radiation from the left portion of the exit pupil does not interfere with the orthogonally polarized radiation from the right portion of the exit pupil. Therefore, the PSF is elongated in the horizontal direction. In this case the PSF is the scalar sum (linear superposition) of two images of a "D" shaped aperture, not the vector sum across the circular aperture shown in the upper right panel in Fig 1. The inner working angle is larger in the horizontal direction than it is for the vertical direction. This means that a coronagraph mask positioned at the image plane that is designed using scalar theory and applied to a system with polarization aberrations would leak large amounts of light around the occulting mask to flood the coronagraph and block light from exoplanets. Unless taken into consideration, this may reduce exoplanet yield to the level of uselessness.

Although this is a rather dramatic example and no one would intentionally place orthogonal linear polarizers over their telescope pupil, this shows that any source of polarization change across the exit pupil will result in distortion of the PSF at some level and may result in light leakage around those occulting masks designed using scalar theory only.

To maximize transmittance and contrast and thus SNR, the coronagraph mask and the Lyot filter need to "impedance" match the complex amplitude (amplitude and phase) electromagnetic field from the star/planet system at the occulting mask.

Fresnel polarization

Here we examine the source of phase and amplitude changes within astronomical telescopes and instruments. Systems require mirrors coated with metals (e.g. Al or Ag) to give high surface reflectance in the visible and thus maximize system transmittance. These mirrors are overcoated with a dielectric material that serves two purposes: 1. A transparent mechanical barrier coat to inhibit oxidation and surface abrasion. 2. Enhance the reflectivity at select wavelengths. In the next section we show that these metal surfaces partially polarize light. These dielectric overcoats contribute by either adding to or subtracting from the polarization aberrations caused by the metal mirror. Dielectric coatings add a degree of complexity that will affect coronagraph contrast and the inner working angle (IWA) and are not discussed here other than to mention they can be used to a limited extent to mitigate polarization aberrations over a small bandwidth in real optical systems.

Broadband unpolarized white-light is a characteristic of nearly all-astronomical sources and is divided equally into two orthogonally polarized beams for the derivation below. We represent unpolarized light by two orthogonal Eigenvector states and, for this example we select linearly polarized Eigenvector states. The Fresnel equations[13,14] are used to model the behavior of a vector electromagnetic complex wave interacting with a metal or dielectric surface (mirror).

A-J Fresnel in 1823 described the theory for interactions of electromagnetic radiation with dielectrics and metals. These relationships were developed further[15] and are the basis of the commercial field of ellipsometry[16]. Here we describe those relationships.

Consider incoherent white-light incident at angle θ_0, onto a metal mirror with isotropic properties. This metal mirror has a wavelength dependent complex index, $N_1(\lambda) = n_1(\lambda) + ik_1(\lambda)$ that is uniform across its surface, and hence called isotropic. The Eigenstates of reflection are the s (perpendicular) and p (parallel) polarized components. A portion of the beam reflects at the incidence angle θ_0 (Snell's Law) and another portion (a damped evanescent wave) penetrates a short distance into the metal at the **complex** refraction angle of θ_1 given by Snell's law[17] and is absorbed to heat the metal. This complex angle is given by

$$\theta_1 = \arccos\left\{\left(\sqrt{N_1^2 - N_0^2 \sin\theta_0^2}\right) / N_1\right\} \qquad \text{Eq 5}$$

The complex reflectivities for light in the p and s polarizations are given by[33]

$$r_p = \frac{\tan(\theta_0 - \theta_1)}{\tan(\theta_0 + \theta_1)} \text{ and } r_s = \frac{\sin(\theta_0 - \theta_1)}{\sin(\theta_0 + \theta_1)} \qquad \text{Eq 6}$$

Two polarization effects occur. 1. A phase shift and 2. A polarization-dependent absorption.

1. Phase Shift

The phase shift occurs between the waves associated with each of the two polarizations. We use the notation to express the angle of retardance of the s-polarized light relative to the p-polarized light. Equation 7 defines the polarization aberration, ψ.

Downloaded From: https://www.spiedigitallibrary.org/conference-proceedings-of-spie on 7/18/2018
Terms of Use: https://www.spiedigitallibrary.org/terms-of-use

$$\tan\psi = \tan\left(\phi_s - \phi_p\right) = \left|r_s\right| / \left|r_p\right|. \quad \text{Eq. 7}$$

Equation 7 gives us the retardance ψ for a single ray propagating through the system. An image requires an array or an ensemble of rays. When we trace multiple rays from a single point in object space, the tangent of the retardance becomes

$$\tan\psi(\xi,\eta) = \tan\left(\phi_s(\xi,\eta) - \phi_p(\xi,\eta)\right) = \left|r_s(\xi,\eta)\right| / \left|r_p(\xi,\eta)\right| \quad \text{Eq. 8}$$

Where (ξ,η) are coordinates across the pupil. And we see that the retardance varies across the pupil, because the angles of incidence of the rays' change.

Polarization dependent absorption

The reflectivity is polarization dependent, with the result that each reflection acts as a partial polarizer. The term diattenuation is used to remind us that there are two (Di) measurements required here. The diattenuation, *D* at each point (ξ,η) across the pupil is given by

$$D(\xi,\eta) = \frac{\left|r_s(\xi,\eta)\right|^2 - \left|r_p(\xi,\eta)\right|^2}{\left|r_s(\xi,\eta)\right|^2 + \left|r_p(\xi,\eta)\right|^2} \quad \text{Eq. 9}$$

Where *r* is the **complex** reflectivity for *s* and *p* light respectfully given in Eq 6 above. Metallic reflection acts as a weak polarizer, and *D* varies from zero, 0, (nonpolarizing) to one, 1, for ideal polarizers. Astronomical optical systems require large étendu (area times solid angle), which requires large optics. However, the volume for spacecraft bus is required to be compact to fit inside launch shrouds. These two requirements conflict and often lead to many fold mirrors in the instrument which, unless designed properly will, in turn, lead to large internal polarization with the concomitant loss in transmission, caused primarily by diattenuation and loss in image quality, caused primarily by retardance.

Note there are two polarization aberrations: 1. Diattenuation is commonly used to model a polarization dependent reflectivity and 2. Retardance is used to model a polarization dependent change in the phase of the complex wave upon reflection.

4. VECTOR -WAVES & POLARIZATION RAY TRACE

Vector wave image formation

In the previous section we examined the scalar diffraction equation 1, above. If the source is partially polarized and the telescope has a polarization dependent transmission, then Eq. 1 is written as:

$$\vec{U}_3(x_3,y_3) = \mathrm{K}\int_{-\infty}^{\infty}\int_{-\infty}^{\infty}[\vec{U}_2^{-}(\xi_2,\eta_2)\vec{\tau}_2(\xi_2,\eta_2)]\cdot\exp\left\{-j\frac{2\pi}{\bar{\lambda}f}(x_3\xi_2 + y_3\eta_2)\right\}d\xi\,d\eta \quad \text{Eq 10}$$

The complex wavefront for unpolarized, incoherent astronomical sources become partially polarized upon propagation through an astronomical telescope and instrument that contains metal mirrors and dielectric surfaces. The Jones matrix[18,19] whose values change for different ray-paths across the exit pupil describes this wavefront. The complex field at each point (ξ,η) across the exit pupil is given by:

$$\left|\begin{array}{cc} A_{XX}e^{i\phi_{XX}} & A_{XY}e^{i\phi_{XY}} \\ A_{YX}e^{i\phi_{YX}} & A_{YY}e^{i\phi_{YY}} \end{array}\right|_{\xi,\eta} = \left|\begin{array}{cc} J_{XX} & J_{YX} \\ J_{XY} & J_{YY} \end{array}\right|_{\xi,\eta} \quad \text{Eq.11}$$

Downloaded From: https://www.spiedigitallibrary.org/conference-proceedings-of-spie on 7/18/2018
Terms of Use: https://www.spiedigitallibrary.org/terms-of-use

On the LHS of Eq. 11, A is amplitude and ϕ is phase of the electric field for each of the 4 component waves in an arbitrarily selected X,Y Eigen basis-set at points ξ,η across the exit pupil. Subscript XX refers to the complex field exiting polarized in X resulting from the incident field with X polarization, as matrix multiplication would imply. A similar convention extends to the subscripts YY, YX and XY. Ideally, the Jones pupil would be the identity matrix for all ray paths and no undesired polarization change would occur[18]. That is, the off-diagonal elements in the matrix shown in Eq. 11 would be zero. During image formation with incoherent light, none of these four Jones pupil components form interference fringes with each other[19,20]. Each is diffracted separately by scalar diffraction theory to calculate the four components of the amplitude response matrix, which is the generalization of the amplitude response function of diffraction theory[21].

The vector transmittance of the telescope $\vec{\tau}_2(\xi_2,\eta_2)$ is written,

$$\vec{\tau}_2(\xi_2,\eta_2)=\left|\begin{array}{cc} J_{XX} & J_{YX} \\ J_{XY} & J_{YY} \end{array}\right|_{\xi,\eta} \qquad \text{Eq 12}$$

The telescope/coronagraph system complex transmittance across the exit pupil depends on the vector of the electromagnetic field at point ξ,η within the exit pupil. The complex electric field $u_3(x_3,y_3)$ at the image plane, for an on-axis unpolarized star of unit brightness follows from the Fresnel Kirchoff diffraction integral and is written:

$$\left.\begin{array}{l} u_3(x_3,y_3)= \\ K\left\{\int_{-\infty}^{\infty}\int_{-\infty}^{\infty}\left|\begin{array}{cc} J_{XX} & J_{YX} \\ J_{XY} & J_{YY} \end{array}\right|\exp\left(-\frac{2\pi}{\lambda f}\left[x_3\xi_2+y_3\eta_2\right]\right)\right\}d\xi d\eta= \\ K\left\{\int_{-\infty}^{\infty}\int_{-\infty}^{\infty}\left[J_{XX}+J_{YY}+J_{YX}+J_{XY}\right]\exp\left(-\frac{2\pi}{\lambda f}\left[x_3\xi_2+y_3\eta_2\right]\right)d\xi d\eta\right\} \end{array}\right\} \qquad \text{Eq. 13}$$

Where *K* is a constant. We assume that the optical power of the system is not vector (polarization) dependent and we have multiplied out the matrix to emphasize that we will discover these 4 terms will be shown to be independent and not correlated.

The amplitude response matrix (ARM) represents the 4 complex amplitude terms at the focal plane, one for each of the 4 Jones pupil elements.

$$u_3(x_3,y_3)=K\left\{\int_{-\infty}^{\infty}\int_{-\infty}^{\infty}\left[\begin{array}{cc} J_{XX} & J_{YX} \\ J_{XY} & J_{YY} \end{array}\right]\exp\left(-\frac{2\pi}{\lambda f}\left[x_3\xi_2+y_3\eta_2\right]\right)\right\}d\xi d\eta=$$

$$\left[\begin{array}{cc} u_{XX}(x,y) & u_{XY}(x,y) \\ u_{YX}(x,y) & u_{YY}(x,y) \end{array}\right]_3=ARM \qquad \text{Eq. 14}$$

To calculate the intensity $I_3(x_3,y_3)$ that we will measure, we take

Downloaded From: https://www.spiedigitallibrary.org/conference-proceedings-of-spie on 7/18/2018
Terms of Use: https://www.spiedigitallibrary.org/terms-of-use

$$I_3(x_3,y_3)=\left|u_3\left(x_3,y_3\right)\right|^2 . \qquad \text{Eq. 15}$$

And from Eq 13, we find the intensity to be

$$I_3(x,y)=$$

$$=\left|u_3\left(x,y\right)\right|^2=\left|K\left\{\int_{-\infty}^{\infty}\int_{-\infty}^{\infty}\left[J_{XX}+J_{YY}+J_{YX}+J_{XY}\right]\exp\left(-\frac{2\pi}{\lambda f}\left[x_3\xi_2+y_3\eta_2\right]\right)d\xi d\eta\right\}\right|^2 \qquad \text{Eq 16}$$

Since we are observing a star, which is a thermal broadband white-light source, it is reasonable to assume that the complex electric fields given by J_{XX}, J_{YY}, J_{YX} and J_{XY} are statistically uncorrelated and therefore incoherent. The cross-product terms within the modulus squared shown in Eq 15 are zero. Consequently, Eq. 15 can be expanded to gives,

$$\begin{aligned} &I_3(x_3,y_3)= \\ &K^2\left|\int_{-\infty}^{\infty}\int_{-\infty}^{\infty}\left[J_{XX}\right]\exp\left(-\frac{2\pi}{\lambda f}\left[x_3\xi_2+y_3\eta_2\right]\right)\right|^2 d\xi d\eta+K^2\left|\int_{-\infty}^{\infty}\int_{-\infty}^{\infty}\left[J_{YY}\right]\exp\left(-\frac{2\pi}{\lambda f}\left[x_3\xi_2+y_3\eta_2\right]\right)\right|^2 d\xi d\eta+ \\ &K^2\left|\int_{-\infty}^{\infty}\int_{-\infty}^{\infty}\left[J_{YX}\right]\exp\left(-\frac{2\pi}{\lambda f}\left[x_3\xi_2+y_3\eta_2\right]\right)\right|^2 d\xi d\eta+K^2\left|\int_{-\infty}^{\infty}\int_{-\infty}^{\infty}\left[J_{XY}\right]\exp\left(-\frac{2\pi}{\lambda f}\left[x_3\xi_2+y_3\eta_2\right]\right)\right|^2 d\xi d\eta \end{aligned} \qquad \text{Eq 17}$$

And we see that we have four point-spread functions, one each for the uncorrelated fields J_{XX}, J_{YY}, J_{YX} and J_{XY} and the image plane point spread function is the linear, incoherent superposition of four PSF's as shown in Eq. 17 below.

$$I_3(x_3,y_3)=\underline{I_3(x_3,y_3)}\big|_{XX}+\underline{I_3(x_3,y_3)}\big|_{YY}+\underline{I_3(x_3,y_3)}\big|_{YX}+\underline{I_3(x_3,y_3)}\big|_{XY} \qquad \text{Eq 18}$$

The subscript XX means X light entering the system polarized in the X direction mapped into the X direction or X<=X, and similarly for light in the Y direction. The subscript XY refers to light entering the system polarized in the Y direction that exits the system in the X direction. Note that at the focal plane the terms $\underline{I_3(x_3,y_3)}\big|_{XX}$ and $\underline{I_3(x_3,y_3)}\big|_{XY}$ are intensities polarized in the X direction and that the terms $\underline{I_3(x_3,y_3)}\big|_{YY}$ and $\underline{I_3(x_3,y_3)}\big|_{YX}$ are intensities polarized in the Y direction.

Polarization ray-trace

The output of a CAD polarization ray-trace computer program (Polaris-M) is combined with Fourier optics to calculate point spread functions. Figure 3 shows a side view of a typical optical system with a fan of rays originating from a point on the object and passing through an optical system with k surfaces to the system exit pupil. Each ray strikes a real physical surface at a known angle of incidence (no paraxial approximation).

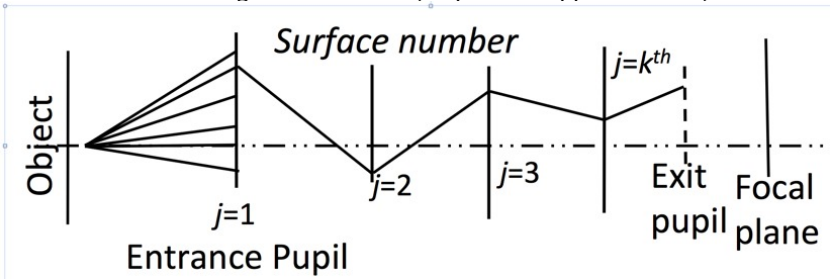

Figure 3 A fan of rays is shown passing from the object plane through an optical system with k surfaces before the exit pupil. For descriptive purposes a fan of rays is shown traced to surface j=1 and then a general single ray continues on to the exit pupil at surface j=k+1.

Downloaded From: https://www.spiedigitallibrary.org/conference-proceedings-of-spie on 7/18/2018
Terms of Use: https://www.spiedigitallibrary.org/terms-of-use

We know the physical properties of each surface. Each surface in an optical system is either a reflecting metal or a dielectric. Using the Fresnel equations, discussed in section 2 we calculate values for each of the four complex entries in Eq. 16, for each ray intercept through the system. We compute the multiplicative amplitude and cumulative phases for both perpendicular and parallel light and map these into four arrays of complex numbers across the exit pupil. We then take a digital FFT of each set of these 4 arrays of complex-field points to calculate the four PSF's.

Polarization ray trace work used for this paper was Polaris-M from Airy Optics[22]

5. LYOT CORONAGRAPH TO CHARACTERIZE EXOPLANETS

Optical schematic

Figure 4 shows the optical path for the complex amplitude and phase as it passes through a typical exoplanet Lyot coronagraph. Several physical optics effects modify this complex wave before it reaches the detector. These are caused by the interaction of light and matter: **polarization** induced by mirrors, windows & stops and **diffraction** produced by masks and stops and **chromatic aberration** which results from the wavelength-dependent indices of refraction of materials required to reflect (metal mirrors) and transmit (dielectrics, filters, prisms, etc.) light.

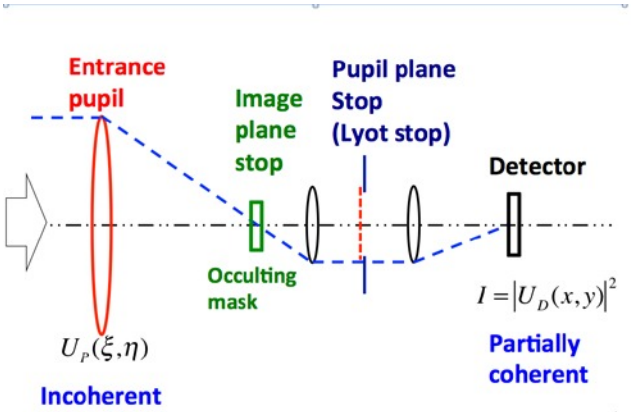

Figure 4. Optical schematic for a typical Lyot coronagraph. The Star/planet complex electromagnetic field enters the Lyot coronagraph system from the left and is focused onto a complex occulting mask located at an image plane stop. This image plane stop is at the front focus of a collimator lens. The optical power on the collimator is such that an image of the entrance pupil field is formed on the Lyot stop. The field is then focused on to the detector. Additional optics (not shown), in particular adaptive optics are inserted before the occulting mask to create a dark hole and the complex wavefront reflects from the several mirrors needed to package the system for flight. By the time light reaches the detector it is partially coherent.

The three-dimensional electric field from exoplanets is thermal white-light broadband, either reflected from the planetary system's parent star or emission from the planet or a mixture. The electric fields associated with the star and the planet are both spatially and spectrally incoherent[23],[24],[25] at the source. This radiation travels through space, enters the telescope/coronagraph system and reflects from several mirrors to strike the occulting-mask stop at an image plane. The field is partially coherent at this stop. The stop must block by absorption or reflection almost all of the incident electric field from the star while passing as much as possible of the exoplanet field. Starlight diffracts around the entrance pupil and this electric field is scattered into the coronagraph to be blocked by the Lyot stop shown in Fig 4. The detector at the focal plane samples the modulus squared of the electromagnetic complex field, which appears as a speckle pattern caused by partial coherence of the wave-fields. This intensity speckle pattern is then digitized at an optimum dynamic range (number of bits) to obtain a high enough SNR for exoplanet characterization.

This intensity distribution contains information about the characteristics of the exoplanet as viewed through the "filter" of the telescope/coronagraph complex-vector transfer function (CVTF). This function, represented by the amplitude response matrix (ARM)[26] varies significantly with the physical optics and the opto-mechanical design implementation.

Downloaded From: https://www.spiedigitallibrary.org/conference-proceedings-of-spie on 7/18/2018
Terms of Use: https://www.spiedigitallibrary.org/terms-of-use

6. THE HabEx POLARIZATION ANALYSIS

Introduction

The optical system for the NASA Habitable Explorer is designed to characterize terrestrial exoplanets using the largest unobscured clear aperture telescope that NASA believes can be manufactured, packaged and launched over the next decade. The opto-mechanical and thin film architecture design was performed by Stefan Martin[27] of JPL to give a geometric-aberration diffraction-limited performance and we were assigned the task to polarization ray trace this design for a detailed performance assessment. Table 7 in that paper provides the HabEx coronagraph instrument parameters. The HabEx Zemax optical prescription, including the opto-mechanical layout of the packaged flight hardware was provided on 5 September 2017 along with a description of the mirror coatings.

HabEx opto-mechanical layout

The next three figures show the end-to-end optical path for the star and exoplanet light traversing through the telescope fore-optics and through the coronagraph instrument to the detector plane.

Figure 5 below shows the first four optical elements in the telescope/coronagraph system. Light from the star and exoplanet enter the system from the lower left, reflect from mirror M1, which is the primary. The beam is converging to a focus when it strikes M2, M3 and M4.

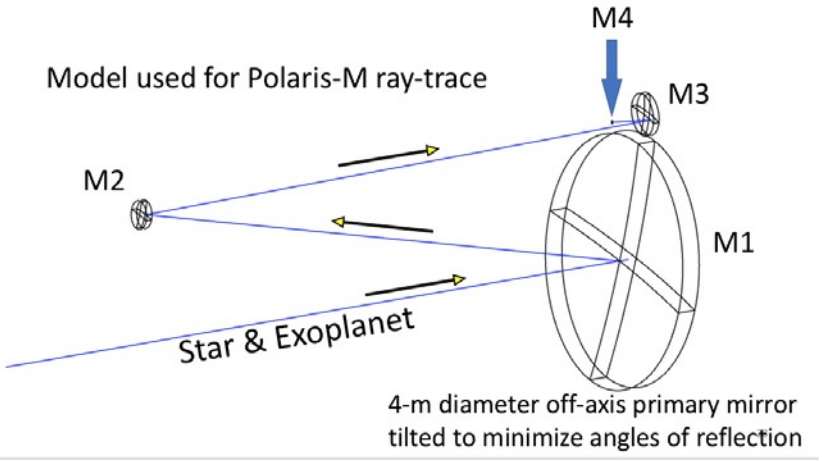

Figure 5 The HabEx primary mirror is a 4-meter off-axis asphere that is tilted relative to its axis to minimize angles of incidence on the primary and thus minimize the polarization aberrations attributable to the primary. Light reflected from the primary reflects from mirrors M2, M3 and M4. Figure 8 below shows where the light goes after striking the small mirror M4.

Figure 6 below shows M4 through M14 of the system. The occulting mask focal plane (OCMFP) is shown. The function of the two deformable mirrors, shown as DM is to create a stable dark hole, using the "Talbot" effect to image block out unwanted light.

Downloaded From: https://www.spiedigitallibrary.org/conference-proceedings-of-spie on 7/18/2018
Terms of Use: https://www.spiedigitallibrary.org/terms-of-use

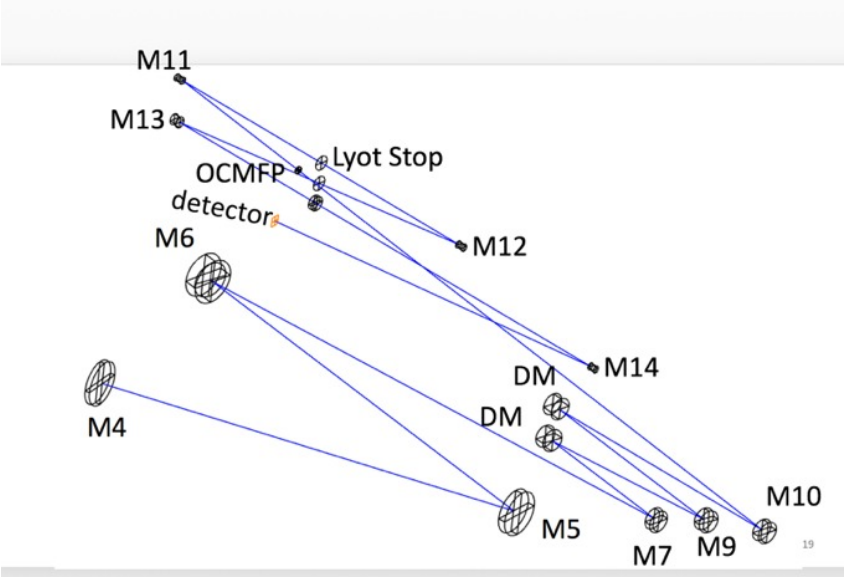

Figure 6 The HabEx telescope/coronagraph system is shown from mirror M4 through to the detector. The initials DM refer to 2 deformable mirrors used create the dark hole for high performance coronagraphy. There are 10 reflections in the system before the occulting mask focal plane.

This HabEx optical prescription is designed to operate at 5 optical wavelengths. These are: 450-550 nm; 551-672 nm; 672-821 nm; 821-1,000 and 950-1,800 nm. We selected the 450 to 550 nm bandwidth to model the polarization properties and image forming performance of Habex. Our experience shows that coatings and image quality performance is most stressed at shorter wavelengths

Coatings analysis:

The highly reflective thin metal films over the curved mirrors, A/O elements and optically flat surfaces have dielectric overcoats to protect from oxidation and maintain high reflectivity during assembly, test, system integration and the mission.

The coating on the first 2 Habex mirrors, that is the 4-meter primary and the secondary is aluminum (Al) with an overcoat of 25-nm MgF2. The polarization aberrations for the remaining mirrors in the complete HabEx optical system are calculated here for two coating recipes': A) Al+25-nm MgF2 (that is the same coating as on the primary & secondary) and B) silver (Ag) over coated with FSS99. We report on the spatial distribution of the diattenuation across the primary mirror and the cumulative diattenuation across the exit pupil to the occulting mask and also, across the exit pupil to the detector, without the occulting mask in the system. Depending on how the occulting mask is fabricated, the polarization properties of the wavefront at the detector may change significantly from those calculated here. Below we show maps of the diattenuation and the retardance across the wavefront as it propagates through the HabEx optical system.

In addition, we present laboratory measurements of the form birefringence across a large (3.75-m) mirror with a "typical" astronomical coating in section 8. These measurements were made by Brian Daugherty[28] and this material is part of his PhD dissertation at the College of Optical Sciences, University of Arizona, Tucson. This coating was made following the processes and procedures used at Kitt Peak National Observatory (KPNO) to coat the 4-meter Mayall telescope. Maps showing changes in retardance and changes in diattenuation across the mirror are presented in Fig and described in section 8.

Figure 7, below shows the cumulative diattenuation maps for two coating recipes on the 11 mirrors just before the exit pupil for the occulting mask. The map on the left is for all 11 mirrors coated with aluminum + 25-nm MgF2 and on the right the diattenuation is calculated under the conditions that mirrors 1 and 2 are coated with Al+25 nm and the remaining 9 mirrors to the exit pupil are coated with Ag+FSS99. These maps are important because they provide an indication of the polarization content of the PSF and enable the thin film engineer to see where on the mirrors the coatings can be changed to optimize the shape of the occulting mask to minimize the diattenuation. We see that by using Ag+FSS99 coating we have reduced the diattenuation by almost a factor of 2. ____

Downloaded From: https://www.spiedigitallibrary.org/conference-proceedings-of-spie on 7/18/2018
Terms of Use: https://www.spiedigitallibrary.org/terms-of-use

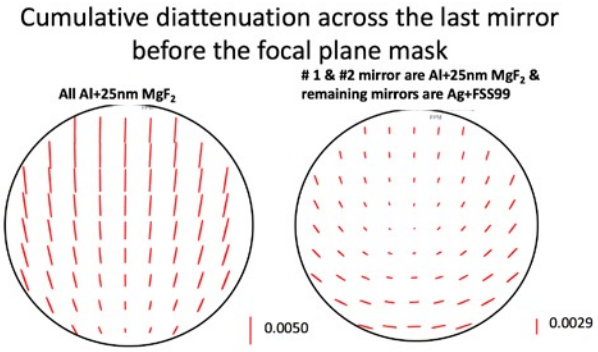

Figure 7 Diattenuation map across the last mirror before the coronagraph occulting focal plane mask in Habex. This was calculated at 500 nm wavelength assuming an ideal thin film reflective coating of evaporated Aluminum, overcoated with a dielectric of 25 nm thick MgF2 on mirrors 1 and 2. The mirrors between #2 and that mirror just before the focal plane mask are assumed to be coated with silver (Ag) overcoated with a dielectric of FSS99. The orientation of the tick marks across the face of the mirror show the preferred polarization vector direction of the reflected light and the length of the tick mark shows the magnitude of the diattenuation. In this case it is 0.0050 for a system where all mirrors are coated with Al+25-nm of MgF2 and the diattenuation is 0.0029 for the case where the first and second mirrors are coated with Al+25nm of MgF2 and the remaining mirrors are coated with Ag+FSS99.

Figure 8 shows the cumulative (primary mirror to coronagraph mask) retardance across the exit pupil to the coronagraph focal plane without the presence of the Lyot occulting mask. In the left panel, we see that If the coatings are Al+25mm MgF_2, we find that the retardance, which changes across the exit pupil is about 0.074 radians or 0.0118 waves. However, examining the right panel in Fig 14 shows that if only mirrors M1 and M2 are Al+25mn MgF2, we find that the retardance exhibits a pattern similar to that shown on the left, but its magnitude is 0.585 radians or .0093 waves at 500 nm which is noticeably less.

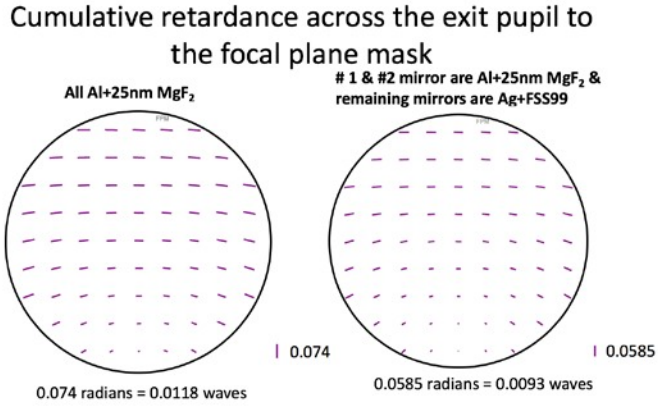

Figure 8 cumulative retardance across the exit pupil to the focal plane mask for the all HabEx mirrors coated with an ideal aluminum plus 25 nm MgF2 (left) and right: for HabEx mirrors 1 & 2 an ideal aluminum plus 25 nm MgF2 and the remaining mirrors silver overcoated with FSS99. Calculated for 500 nm.

Diattenuation & retardance interpretation & summary analysis

We calculated the polarization aberrations: diattenuation and retardance and showed the spatial dependence of these aberations across the three surfaces: 1. The primary mirror, 2. The exit pupil to the coronagraph occulting mask and 3. The exit pupil to the coronagraph image plane without the presence of an occulting mask.

Compare the 2 mirror coatings: A. All Al+25nm MgF2 and B. #1 & #2 mirror coated with Al+25nm MgF2 with the remaining mirrors Ag + FSS99. It appears that coating system B shows lower diattenuation and lower birefringence than does coating system A.

It is our understanding that the base-line coatings are now Al+25nm MgF2 on mirrors 1, 2 and 3, and we continue our analysis under that assumption.

Downloaded From: https://www.spiedigitallibrary.org/conference-proceedings-of-spie on 7/18/2018
Terms of Use: https://www.spiedigitallibrary.org/terms-of-use

7. HebEx JONES PUPIL

Background

The HabEx image of the star and its planetary system at the occulting mask must match the complex transmittance of the occulting mask to achieve optimum attenuation. The quality of the Habex image is shown in the Jones pupil at the exit pupil to the occulting mask image plane. The complex wavelength as a function of wavelength and field $u(\xi,\eta;\lambda)$ across the exit pupil is given by

$$u(\xi,\eta;\lambda)=\begin{bmatrix} A_{XX}(\xi,\eta)e^{i\phi_{XX}(\xi,\eta)} & A_{XY}(\xi,\eta)e^{i\phi_{XY}(\xi,\eta)} \\ A_{YX}(\xi,\eta)e^{i\phi_{YX}(\xi,\eta)} & A_{YY}(\xi,\eta)e^{i\phi_{YY}(\xi,\eta)} \end{bmatrix}_{\lambda} \quad \text{Eq. 19}$$

To display the spatial distribution of amplitude and phase across the Jones pupil we partition them as shown below.

$$\text{Amplitude}=\begin{bmatrix} A_{XX}(\xi,\eta) & A_{XY}(\xi,\eta) \\ A_{YX}(\xi,\eta) & A_{YY}(\xi,\eta) \end{bmatrix} \quad \text{Eq. 20}$$

and the phase changes across the Jones pupil are shown as

$$\text{Phase}=\begin{bmatrix} \phi_{XX}(\xi,\eta) & \phi_{XY}(\xi,\eta) \\ \phi_{YX}(\xi,\eta) & \phi_{YY}(\xi,\eta) \end{bmatrix} \quad \text{Eq. 21}$$

The Jones pupil across the exit pupil to the occulting mask tells us the shape of the PSF and its polarization content at the occulting mask. The following figures show the amplitude and phase of the Jones pupil for HabEx as it appears across the exit pupil to the occulting mask at wavelength 550 nm.

Downloaded From: https://www.spiedigitallibrary.org/conference-proceedings-of-spie on 7/18/2018
Terms of Use: https://www.spiedigitallibrary.org/terms-of-use

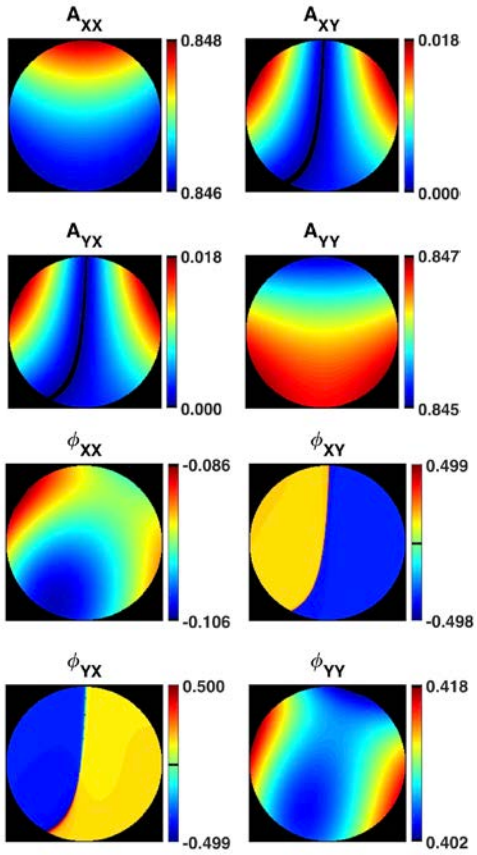

Figure 9 Jones exit pupil (ξ,η) as observed from the occulting mask for the HabEx at 500-nm wavelength. Top four: Color scale shows amplitude reflectance as a function of position across the exit pupil. Bottom 4: Color scale shows phase as a function of position across the exit pupil

Figure 9 shows the Jones exit pupil (ξ,η) as viewed looking back into the optical system. The top four panels show the amplitude of the Jones pupil. For A_{XX} and A_{YY}, we see insignificant changes across the pupil for the amplitude reflectance of the system and that the intensity transmission of the system is 71%, for approximately 30% absorption before the occulting mask. The off-diagonal elements, A_{XY} and A_{YX} of the amplitude part of the Jones pupil are very small, but make a contribution to light at the coronagraph focal plane[27].

The phase part of the Jones pupil is shown in the lower four images in Fig. 16. In the figure labeled ϕ_{XX} we see that the local wavefront error varies across the pupil by 0.02 waves at 500 nm. In the figure labeled ϕ_{YY} we see that the local wavefront error varies across the pupil by 0.02 waves at 500 nm. Both exhibit the same sign. Looking at the shape of the wavefront across the exit pupil it appears that a small amount of the geometric wavefront astigmatism will provide a level of correction. This needs to be investigated further.

The phase terms ϕ_{XY} and ϕ_{YX} of the Jones pupil exhibit a 2 π phase change. Because the amplitudes A_{XY} and A_{YX} are so small we ignore the phase terms ϕ_{XY} and ϕ_{YX} in this work.

Adaptive optics challenge

The exit pupil to the coronagraph occulting mask contains two superposed co-propagating complex wavefronts, of nearly equal amplitude. However, the retardance between them and the shapes of the two accompanying phase distributions are different. This is shown in Fig 17 where the pair of images at the top represent the amplitude and phase distributions across the exit pupil for XX light and the pair of images at the bottom represent the amplitude and phase distributions across the exit pupil for YY light.

Adaptive optics corrects geometric wave aberrations and is not sensitive to the polarization content of the radiation striking it. Consequently, classic adaptive optics cannot correct for both sets of wavefront errors simultaneously. These polarization-induced wavefront-error differences need to be corrected up-stream in the optical system by rebalancing polarization and geometric wavefront aberrations before the occulting mask.

Downloaded From: https://www.spiedigitallibrary.org/conference-proceedings-of-spie on 7/18/2018
Terms of Use: https://www.spiedigitallibrary.org/terms-of-use

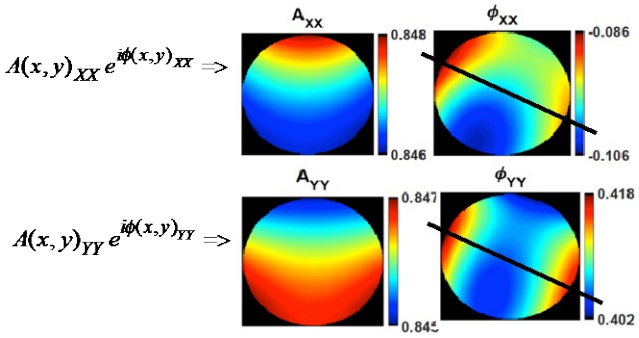

Fig 10. The pair of images at the top represent the amplitude and phase distributions across the exit pupil for XX light and the pair of images at the bottom represent the amplitude and phase distributions across the exit pupil for YY light. The amplitude scale is electric field and the phase scale is waves at 500 nm wavelength. The black lines across the phase images show the direction of the slice taken to calculate the optical phase differences shown in Fig 11 below.

Phase difference

Based on the work of others[29,30], it is clear that A/O is an essential part of making exoplanet coronagraphs work at their required contrast level. The first step in mitigating this aberration is to examine, in detail the magnitude and sign of the error and next to develop technology to minimize the effect.

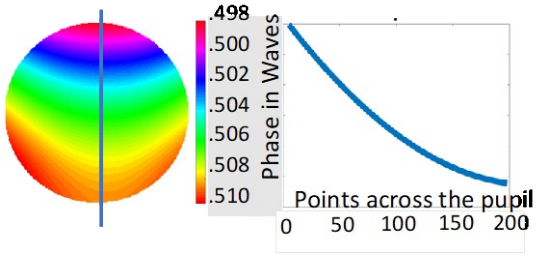

Figure 11 Left: difference in phase between $\phi_{XX}(\xi,\eta) - \phi_{YY}(\xi,\eta)$, with vertical line showing slice for the curve on the right. Right: phase difference in waves at 500 nm as a function of position along the line straight line shown on the left, is presented on the right.

In Fig 18, we see that there is approximately 0.5 waves retardance between the two phase-planes and that this retardance varies between 499 and 509 mili waves across the exit pupil. An A/O system can correct one polarization-state wavefront OR the orthogonal polarization-state wavefront, but NOT both simultaneously.

The current HabEx optical prescription cannot effectively utilize A/O. Therefore, the analysis developed by J. Davis, et. al.[8,32] and printed as 10698-120 shows calculations of Normalized Polychromatic Irradiance without adaptive optics.

Downloaded From: https://www.spiedigitallibrary.org/conference-proceedings-of-spie on 7/18/2018
Terms of Use: https://www.spiedigitallibrary.org/terms-of-use

8. ANISOTROPIC THIN FILMS

Measurements of Form Birefringence across a 3.75-meter mirror

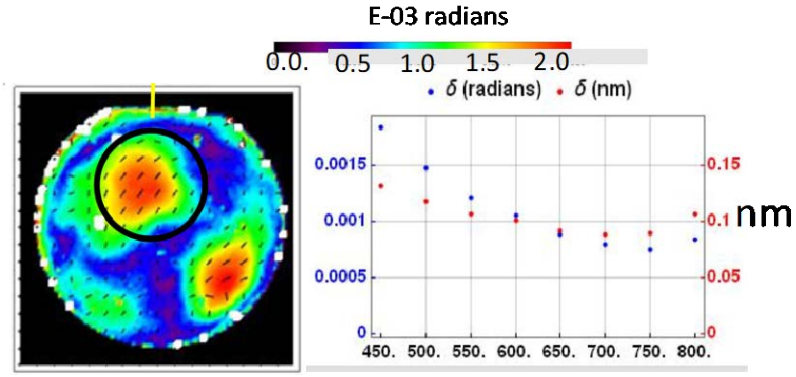

Fig 12. Left: Color, coded map of the form birefringence, in units of 10-3 radians of retardance across the 3.75 meter spherical optical test mirror used at the University of Arizona mirror lab to fabricate the segments of the Giant Segmented Mirror Telescope (GSMT). Right, plot of the retardance in both units of radians (left) and nm as a function of wavelength from 450 to 800 nm. This retardance has no affect on the mirror's ability to provide precision wavefront accuracy for testing the GSMT, but this retardance does affect exoplanet coronagraphy. Measurement method and processes were developed, hardware built and measurements were made by B. Daugherty[31]

Davis, Et. al. [32] show a detailed polarization ray-trace analysis of the complete HabEx telescope/coronagraph system incorporating a VV6 coronagraph mask and 0.90 Lyot field stop. These authors examined the effects of form birefringence on coronagraph contrast and report that to avoid polarization aberrations that will affect coronagraph contrast the primary mirror needs to be specified at manufacture for minimum or no form birefringence across its large area surface.

9. CONCLUSION

We polarization raytraced the Sept 2017 prescription for the HabEx Lyot coronagraph optical system without an occulting mask and we investigate the physical nature of the electric field at the exit pupil (Jones pupil). We discovered that the shapes of the electric fields across the exit pupil for XX polarized light is different than that for the YY polarized light. The phase difference is about 10 milliwaves, which is too large to be easily corrected efficiently. The opto-mechanical layout, and coatings need to be adjusted to see if a solution using both dual-polarization plane wavefronts is achievable to obtain maximum exoplanet contrast with maximum system transmittance.

The primary mirror needs to be specified at manufacture for minimum or no form birefringence.

8. ACKNOWLEDGEMENTS

This work was supported in part by NASA TDEM15 research grant #NNX17AB29G awarded by the NASA Science Mission Directorate to James Breckinridge, PI, at the College of Optical Sciences at the University of Arizona.

REFERENCES

[1]J. B. Breckinridge, T. G. Kuper and R. V. Shack (1984) "Space telescope low scattered light camera: a model," Optical Engineering, 23, 816-820. also Proc. SPIE 331, 395-403, 1982.

[2] J. B. Breckinridge and B. Oppenheimer (2004), "Polarization Effects in Reflecting Coronagraphs for White Light Applications in Astronomy," ApJ, 600, pp 1091 – 1098.

[3] J. B. Breckinridge, W.S.T. Lam and R. A. Chipman (2015) "Polarization aberrations in astronomical telescopes" Publ. Astron Soc. Of the Pacific 127:445-468

[4] R. A. Chipman, Wai Sze T. Lam and J. Breckinridge (2015) "Polarization aberrations in astronomical telescopes" Proc SPIE 9613 doi:10.1117/12.2188921

Downloaded From: https://www.spiedigitallibrary.org/conference-proceedings-of-spie on 7/18/2018
Terms of Use: https://www.spiedigitallibrary.org/terms-of-use

[5] N. Zimmerman, A. J. E. Riggs, N. J. Kasdin, et. al. (2016) "Shaped pupil coronagraphs: high contrast solutions for restricted focal planes", JATIS 2, 011012
[6] H. Tang, M. Rud, R. Demers, R. Goullioud, et. al. (2015) "The WFIRST/AFTA Coronagraph Instrument Optical Design", Proc. SPIE **9605** 960504
[7] K. Balasubramanian, S. Shaklan, A. Give'on, E. Cady and L. Marchen (2011) "Deep UV to NIR space telescopes and exoplanet coronagraphs: a trade study on throughput, polarization, mirror coating options and requirements" Proc. SPIE 8151 51511G
[8] The vector vortex analysis of HabEx is presented in the paper # J. Davis, M. Kupinski, J. Breckinridge, and R. Chipman: **HabEx polarization ray trace and aberration analysis** Paper 10698-120.
[ix] Joseph W. Goodman (2005) "Fourier Optics" Roberts and Company book ISBN 9747077-2-4
[x] J. D. Gaskill (1978) "Linear Systems, Fourier ransforms and Optics", John Wiley & Sons, NY 400 pages.

[11] Harrington, DM (Harrington, David M.)[1,2,3]; Kuhn, JR (Kuhn, Jeffrey R.)[4]; Ariste, AL (Ariste, Arturo Lopez)[5] **(2017)** Daytime sky polarization calibration limitations, JATIS **3**; DOI: 10.1117/1 JATIS.3.1.018001

[12] Canovas, H.; Rodenhuis, M.; Jeffers, S. V.; et al. (2011) "Data-reduction techniques for high-contrast imaging polarimetry Applications to ExPo", A & A 531 #A102 DOI: 10.1051/0004-6361/201116918
[13] Born, M. & E. Wolf (1993) "Principles of optics", Pergamon Press– Fresnel Equations are derived on pp 627-633
[14] L. Ward (1988) "Optical Constants of Bulk Materials and Films", Adam Hilger, Bristol and Philadelphia, 245 page book.
[15] A. Thelen, (2002) "Design of Optical Interference Coatings" (McGraw-Hill, New York, 1988). AND H. A. Macleod, "Thin-Film Optical Filters" Institute of Physics, pp. 185–186. AND J.A. Dobrowolski, "Coatings and Filters," in Handbook of Optics, W.G. Driscoll and W. Vaughan, ed.(1978) (McGraw-Hill, New York), 8.1-8.124.
[16] R. M. A. Azzam and N. M. Bashara (2003) "Ellipsometry and Polarized Light", North Holland – Elsevier ISBN 0 4444 87016 4 ; 527 pages.
[17] Ward, L. 1988, "Optical Constants of Bulk Materials and Films", Adam Hilger, p245
[18] R. C. Jones, (1941) JOSA, 31, 488
[19] E. Wolf (2007) "Theory of Coherence and Polarization of Light", Chapter 8, Cambridge University Press, 225 page book. And J. W. Goodman (2015) "Statistical Optics", Wiley. And J. D. Strong (1958) "Classical Optics", Freeman, page 178 interference of polarized light,.
[20] E. Wolf (2007) "Theory of Coherence and Polarization of Light", Chapter 8, Cambridge University Press, 225 page book. And J. W. Goodman (2015) Statistical Optics, Wiley And J. D. Strong (1958) Classical Optics, Freeman, page 178 interference of polarized light,.
[21] J.P. McGuire, Jr., R.A. Chipman (1990) "Diffraction image formation in optical systems with polarization aberrations I: Formulation and example", Journal of the Optical Society of America A., vol. 7, no. 9, pp. 1614-1626 (Sept. 1990).
[22] Airy Optics http://xxx.airyoptics.com/, Accessed: 2018-05-16
[23] M. Born and E. Wolf (1999) "Principles of Optics", Chapter 10: Partially coherent light, Cambridge University Press
[24] L. Mandel and E. Wolf (1965) "Coherence Properties of Optical Fields", Rev. Mod. Phys **37**, 231-280
[25] J. Goodman (2015) "Statistical Optics" Ch 5: Coherence of Optical Waves, Wiley and Sons publisher
[26] J. Breckinridge, T. Lam and R. Chipman (2015) "Polarization Aberrations in Astronomical Telescopes: The Point Spread Function", Publications of the Astronomical Society of the Pacific (PASP), 127:445–468. Equation 8
[27] Stefan Martin, Mayer Rud, Paul Scowen, Daniel Stern, Joel Nissen, John Krist (2017), HabEx Space Telescope Optical System. Proceedings of the SPIE, Vol 10398 Paper # 05
[28] B. J. Daugherty, PhD dissertation U of A 2018.
[29] Bowler, B. P. "Imaging extrasolar Giant Planets" Pub. Astron. Soc. Pacific 128, 102001 (2016
[30] Mawet, D. Wizinowich, P. Dekany, R. Keck Planet Imager and characterizer: concepts and phased implementation SPIEProc. 9909, paper 0D. 2016.
[31] B. Daugherty (2018) "Demonstration of a form birefringence measurement methodology for large mirrors", University of Arizona, PhD dissertation
[32] J. Davis, M. Kupinski, R. Chipman and J. Breckinridge, (2018) **"**HabEx polarization ray trace and aberration analysis" Paper 10698-120 SPIE Proceedings paper # 10698-120

Downloaded From: https://www.spiedigitallibrary.org/conference-proceedings-of-spie on 7/18/2018
Terms of Use: https://www.spiedigitallibrary.org/terms-of-use